Coherent Anti-Stokes Raman Scattering Microscopy of Samples Probed with Gaussian Volumes

Michele Marrocco*

ENEA, via Anguillarese 301, S. Maria di Galeria, Rome, Italy

Received: July 3, 2008; Revised Manuscript Received: October 20, 2008

Coherent anti-Stokes Raman scattering (CARS) microscopy is becoming increasingly popular to characterize biochemical samples. Within this context, we show that theoretical analysis can still be accomplished under the simple assumption of Gaussian volumes instead of spatial shapes obtainable from diffraction necessary to describe the tight-focusing condition realized within the focus of microscopes with high numerical apertures. The assumption, common in other physical and chemical spectroscopic techniques based on microscopy (e.g., fluorescence correlation spectroscopy, photon counting histogram) and never applied to CARS, is here used to determine the expression of the anti-Stokes electric field. Contrary to the standard approach resorting to numerical methods, we find that either the field is analytical for certain shapes of the Raman scatterer or the numerical reconstruction is strongly limited. In addition, we examine tests against two typical problems found in the literature, namely, a description of CARS radiation patterns and CARS imaging. With regard to the latter, we remark that the loss of spatial symmetry, the treatment of which is onerous in standard CARS microscopy because of possible separations between the microscope focus and the Raman scatterer, can be handled with ease in the limit of Gaussian volumes. An example is considered for polystyrene beads that are usually employed as test model of a CARS response of relevant biochemical samples.

1. Introduction

Coherent anti-Stokes Raman scattering (CARS) microscopy, or microCARS, is rapidly being recognized as one of the most advanced spectroscopic techniques available to probe matter of chemical and biological interest.[1−4] This is made possible by the advantageous properties of four-wave mixing processes occurring when electromagnetic waves traverse a medium.[5] In more detail, CARS is rooted in the interaction of three incident electric fields with Raman resonances of molecules that can be polarized so effectively that a fourth field is produced at anti-Stokes frequencies.[5] This new field carries the molecular optical response that is rich in information on various biochemical phenomena, the observation of which can be realized at the focus of microscopes with high numerical apertures (NAs).[1−4] However, although CARS microscopy is nowadays a credit to the specialist of spectroscopic applications in physical chemistry,[1−4] the generation of CARS signals for studies of microscopy was pioneered much earlier than its widespread importance.[6] It was indeed not until recently that the advantages of microCARS were clearly demonstrated.[7] These include molecular selectivity, high spatial resolution, three-dimensional sectioning, high optical collection efficiency, and fluorescence-free background. It is then not surprising that, in the past decade, the potential of CARS has been explored in so many works that the subject is already mature for extensive reviews.[1−4]

Rivaling microCARS, techniques based on fluorescence microscopy benefit from the so-called three-dimensional Gaussian (3DG) approximation.[8−10] Introduced more than 30 years ago in a study of fluorescence correlation spectroscopy (FCS),[11] the approximation dictates that the detected volume within the focus of a microscope be modeled by means of Gaussian profiles instead of the spatial shapes obtained with the help of diffraction theory.[12] The approximation is, for example, a milestone in FCS and photon counting histogram analysis.[8−11,13] Furthermore, its use has proven to be valid in the recently founded technique of CARS correlation spectroscopy (where, however, the theoretical interpretation of experimental data is restricted to completely phase-matched signals only).[14,15] Nonetheless, it is striking that the role of the 3DG approximation has not yet been considered in the general theory of microCARS.

Fulfilling this gap, here, we show the physical basis of the approximation in relation to the description of the emitted radiation at anti-Stokes frequencies. More importantly, we will see that theoretical CARS imaging can be accomplished in a manner that is greatly simplified by comparison with the common approach, where everything is treated numerically. But, before going through the details of the main argument of this article, it is necessary to briefly review the basic elements of the problem in order to let the general reader grasp the complexity involved in the physics of CARS microscopy.

2. CARS Microscopy Based on Diffraction Theory

The essence of the central problem faced in microCARS revolves around two cornerstones of optical physics.[1−4] One is the description of a diffraction-limited focus of a microscope with a high NA.[12] The other regards the generation of an anti-Stokes electric field $\mathbf{E}_{aS}$, which stems from the Maxwell equations describing the third-order nonlinear polarization created by the propagation of three electromagnetic waves through the Raman medium.[5] The combination of these two approaches is extremely powerful, but the drawback is that numerical calculation of several integrals is unavoidable. This difficulty can be illustrated by considering both the diffraction pattern of the focused laser light and the solution $\mathbf{E}_{aS}$ of the Maxwell equations in terms of scalar Green's functions.[1,16,17]

* Author to whom correspondence should be addressed. Tel.: +39 06 3048 3345. Fax: +39 06 3048 4811. E-mail: michele.marrocco@casaccia.enea.it.

10.1021/jp805869s CCC: $40.75
Published on Web 11/24/2008

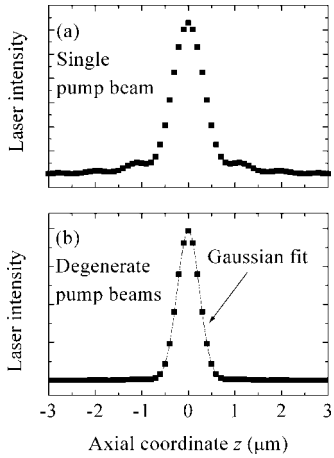

Figure 1. Axial distribution of focused laser intensity for a single beam (panel a) and two degenerate beams (panel b). The laser beam waist is assumed equal to the dimension of the microscope back aperture. The numerical aperture NA is 1.4.

Very concisely, the microscope of focal length f is conceptualized in agreement with diffraction theory,[12] which prescribes that an incident field, linearly polarized along the x axis and propagating along the z axis, is focused as

$$\mathbf{E}_j(\rho,\phi,z)=\frac{ik_jf\exp(-ik_jf)}{2}\begin{bmatrix}I_{00}+I_{02}\cos 2\phi\\ I_{02}\sin 2\phi\\ -i2I_{01}\cos\phi\end{bmatrix} \quad (1)$$

where the index j takes on respectively the symbol p or S for pump and Stokes lasers, k_j is the associated wave vector amplitude, φ is the angle of the cylindrical coordinates of $\mathbf{E}_j$, and finally the integrals I_{0m} are given by[18]

$$I_{0m}=\int_0^{\alpha_{max}} E_j^{inc}(\alpha)\, g_m(\alpha)\, J_m(k_j\rho\sin\alpha)\exp(ik_jz\cos\alpha)\,d\alpha \quad (2)$$

In eq 2, α is the incident angle with maximum value $\alpha_{max}=\sin^{-1}(\mathrm{NA}/n)$; $g_m(\alpha)$ equals $\sin\alpha\sqrt{(\cos\alpha)}(1+\cos\alpha)$, $\sin^2\alpha\sqrt{(\cos\alpha)}$, or $\sin\alpha\sqrt{(\cos\alpha)}(1-\cos\alpha)$ for $m=0$, 1, and 2; and $J_m(k_j\rho\sin\alpha)$ indicates the Bessel functions depending on the radial coordinate ρ. The incident field $E_j^{inc}(\alpha)$ appearing in I_{0m} is calculated at the back aperture of the microscope lens as

$$E_j^{inc}(\alpha)=E_{j0}\exp(-f^2\sin^2\alpha/w_0^2) \quad (3)$$

with w_0 being the laser beam waist before the aperture.

Eqs 1−3 recapitulate the essential knowledge needed to determine the laser focus, and having clarified this, we can now concentrate on the second part of the calculation concerning the anti-Stokes field $\mathbf{E}_{aS}$. Although its general expression can be found in the literature,[1] we take instead the common view of linearly polarized focused fields interacting with a homogeneous Raman medium.[1,2] In this manner, the anti-Stokes field at position $\mathbf{R}=R[(\sin\Theta)(\cos\Phi),(\sin\Theta)(\sin\Phi),\cos\Theta]$, and for each possible state of polarization $\mathbf{e}_q$ ($q=1,2$) becomes[17]

$$\mathbf{E}_{aS}^{(q)}(\mathbf{R})=-\mathbf{e}_qS_qu_R\chi^{(3)}\int_{Vol}E_p^2(\mathbf{r})\,E_S^*(\mathbf{r})\times\exp(-ik_{aS}\mathbf{R}\cdot\mathbf{r}/R)\,d\mathbf{r} \quad (4)$$

where the integral runs over the volume of the Raman source. In eq 4, the nonlinear optical susceptibility, responsible for the CARS signal, is indicated with the usual notation $\chi^{(3)}$, whereas the function u_R represents the spherical wave and the function S_q is $S_1=\sin\Phi$ or $S_2=(\cos\Theta)(\cos\Phi)$, in accordance with the state of polarization of the emitted light. The main calculation is finally completed by considering the field intensity

$$I_{CARS}=\varepsilon_0cn|\mathbf{E}_{aS}(\mathbf{R})|^2/2 \quad (5)$$

that can be used for further elaboration of microCARS signals.

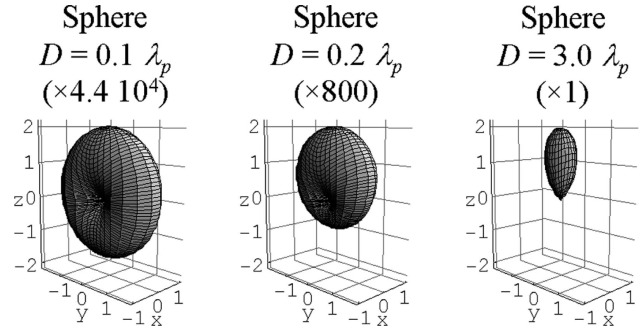

Figure 2. MicroCARS radiation pattern based on eq 9 for a Raman sphere of different diameters D. In agreement with ref 1, the spatial scales of each plot have been normalized to half of the maximum amplitude of the result obtained for $D=3\lambda_p$ (the spatial rescaling is indicated between parentheses). Optical parameters are identical to the calculation of Figure 3a of ref 1.

3. CARS Microscopy with a Gaussian Focus: Radiation Pattern

The immediate conclusion of the previous summary is that the whole calculation cannot be carried out by means of analytical tools. In particular, the integrals of eqs 2 and 4 are so problematic that a full numerical treatment is inescapable. It is then natural to ask to what extent the 3DG approximation can be used to simplify the problem at hand.

Let us first note that the approximation was recently scrutinized in detail, and it was found that its use in multiphoton spectroscopy is highly reliable.[19,20] This finding can be justified with the help of Figure 1, where the axial profile of the laser focus is evaluated according to eqs 1−3 for a microscope of NA = 1.4. As apparent, the case of two degenerate laser beams, that is, Figure 1b, can be precisely simulated by a Gaussian curve. By contrast, this is not possible in Figure 1a, which is distinguished from Figure 1b by the diffraction pattern appearing at the base of the main lobe. The physical explanation of Figure 1 is very simple. In multiwave (or multiphoton) processes, the interaction rescales with the power law characterizing the processes under study, and for this reason, the importance of diffraction is practically reduced in comparison with the role played by the main spatial peak. This observation is not confined to degenerate CARS because its validity is very general and holds for any frequency combination of the laser beams, although experimental realizations with two degenerate pump beams and one Stokes laser in a collinear geometry are the most common. As a consequence, in CARS microscopy, the main contribution to the signal could be easily understood in terms of Gaussian-shaped laser foci instead of the accurate (but lengthy) determination based on eqs 1−3.

To verify this hypothesis, we will examine the well-known case of a Raman medium accommodated in a sphere of variable diameter $D=2\delta$ and placed exactly at the microscope focus.[1−3] The spatial widths of the focused laser beams are assumed to be identical for the sake of simplicity and are defined by w_g in the radial plane and z_g in the axial direction. For the most typical laser configuration (degenerate pump beams copropagating with the Stokes beam), the three-dimensional integral of eq 4 reduces to

$$\int_{\text{Sphere}} E_{\text{p}}^2(\mathbf{r})\, E_{\text{S}}^*(\mathbf{r}) \exp(-ik_{\text{aS}}\mathbf{R}\cdot\mathbf{r}/R)\, \mathrm{d}\mathbf{r} = \frac{2\sqrt{3}}{3}\pi^{3/2} z_g \delta^2\, E_{\text{p}}^2(0)\, E_{\text{S}}^*(0)\, F(\Theta) \quad (6)$$

where the wave vector mismatch $\Delta k = k_{\text{aS}} \cos\Theta - 2k_{\text{p}} + k_{\text{S}}$ influences the argument of Gaussian functions (instead of Sinc functions as in ordinary CARS[5]) according to

$$F(\Theta) = \exp[-(z_g \Delta k)^2/12]\, b(\Theta) \quad (7)$$

with the function $b(\Theta)$ limiting the entire calculation to one integral only, that is,

$$b(\Theta) = \int_0^1 \eta J_0(k_{\text{aS}}\delta\eta \sin\Theta) \times \exp[-3(\delta\eta/w_g)^2]\, \mathrm{Re}\{\mathrm{Erf}[\xi(\eta)]\}\, \mathrm{d}\eta \quad (8)$$

which depends on the detection angle Θ through both the Bessel function J_0 and the complex function $\xi(\eta)$, defined as follows: $\xi(\eta) = \sqrt{3}[\delta\sqrt{(1-\eta^2)}/z_g + iz_g\Delta k/6]$.

Having simplified the calculation of the CARS field so much, we can finally give the result

$$\mathbf{E}_{aS}^{(q)}(\mathbf{R}) = -\frac{2\sqrt{3}}{3}\pi^{3/2} S_q u_R \chi^{(3)} z_g \delta^2\, E_{\text{p}}^2(0)\, E_{\text{S}}^*(0)\, F(\Theta)\, \mathbf{e}_q \quad (9)$$

The handling of eq 9 is now much easier than the complete set of integrals needed to provide the anti-Stokes field in ordinary microCARS.[1−4] An example is the solution of eq 9 in the limit of a very small sphere ($D \ll \lambda_p$). In this case, the phase matching, determined by the wave vector difference Δk, disappears in eq 7, which is transformed into $F(\Theta) = 2\delta/[\sqrt{(3\pi)}z_g]$. This means that the field becomes analytical and is written as

$$\mathbf{E}_{\text{aS}}^{(q)}(\mathbf{R}) = -V_{\text{Sphere}} S_q u_R \chi^{(3)}\, E_{\text{p}}^2(0)\, E_{\text{S}}^*(0)\, \mathbf{e}_q \quad (10)$$

where $V_{\text{Sphere}} = 4\pi\delta^3/3$ is the spherical volume of the Raman scatterer. It is instructive to observe that this result explains why the phase matching is meaningless when the Raman source is smaller than the relevant wavelengths involved in the problem. This fact is very well known as relaxation of the phase matching condition and was theoretically investigated previously with numerical methods only.[1,2,21] However, eq 10 provides a way to demonstrate the relaxation along analytical lines.

As a further example of such a simplified approach, Figure 2 shows the angular distribution of the CARS radiation, or radiation pattern, for different diameters ($D = 0.1, 0.2, 3.0\lambda_{\text{p}}$) of the Raman sphere. All of the numerical values of the remaining optical parameters have been taken from the fundamental works of Cheng et al. in ref 1 or Cheng and Xie in ref 2 in order to directly compare their results (i.e., Figure 3 of ref 1 or Figure 5 of ref 2) with Figure 2 based on eq 9. To that end, the normalization of the spatial scales in the three-dimensional plots of Figure 2 has been chosen in agreement with the published results of Cheng et al. As seen in the comparison, the simplified approach is capable of illustrating the main features of the far-field CARS radiation pattern. First of all, the relaxation of the phase-matching condition for a small Raman source ($D = 0.1\lambda_{\text{p}}$) is readily identified and implies that forward and backward CARS are practically symmetric. On the other hand, the symmetry starts to break for a slightly larger diameter of the spherical Raman sample ($D = 0.2\lambda_{\text{p}}$). In this instance, the main contribution to the emitted radiation stems from forward CARS, whereas backward radiation tends to decrease and becomes negligible for larger scatterers (e.g., $D = 3.0\lambda_{\text{p}}$).

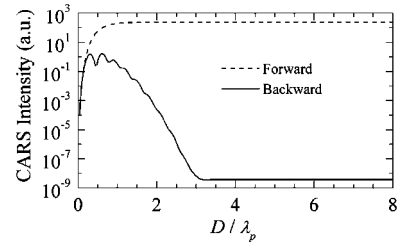

Figure 3. Comparison between forward and backward CARS microscopy depending on the diameter of the Raman sphere. The other physical parameters are taken from Figure 2.

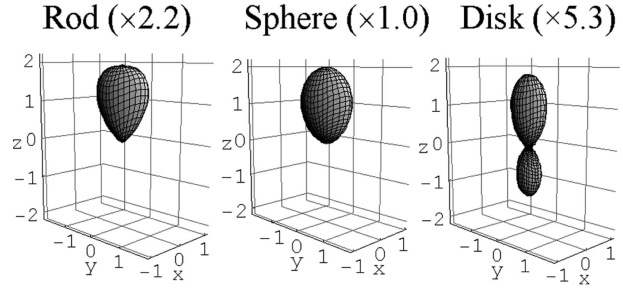

Figure 4. MicroCARS radiation pattern based on eq 9 for three different geometries of the Raman source. In agreement with ref 1, the spatial scales of each plot have been normalized to half of the maximum amplitude of the result obtained for the sphere (the spatial rescaling is indicated between parentheses). The z axis (axial direction) corresponds to the vertical axis of the figures. Optical parameters are identical to the calculation of Figure 3b of ref 1.

Having explained the qualitative changes of the radiation pattern of Raman spheres, it should be pointed out that the plot for $D = 0.2\lambda_{\text{p}}$ also quantitatively corresponds to the equivalent result obtained by means of the full numerical treatment based on diffraction theory (the spatial rescaling of 800 is unaltered between the plot of Figure 2 and the plot of Figure 3a in ref 1 or Figure 5a in ref 2). However, if the spatial rescaling of the calculated patterns obtained for $D = 3.0\lambda_{\text{p}}$ is unitary by definition, it must be observed that, as to the intensity amplitudes, very small scatterers ($D = 0.1\lambda_{\text{p}}$) show substantial disagreement with the parallel result of refs 1 and 2. In the approximated calculation of Figure 2, the rescaling for $D = 0.1\lambda_{\text{p}}$ is, indeed, more than 2 times larger than the analogous value found within the realm of diffraction theory (i.e., 4.4×10^4 against 1.9×10^4), meaning that the prediction based on the 3DG approximation underestimates the CARS intensities of very small Raman spheres.

Apart from this flaw, it is undoubtedly true that the behavior represented in Figure 2 brings out one of the known differences between detection schemes based on the so-called forward CARS (F-CARS) and backward or epidetected CARS.[1−4] But, in view of a deeper comparison with published results, the investigation can be extended to the different progressions of the integrated signals as functions of the sphere size. The integration is realized over the solid angle permitted by the microscope lens (NA = 1.4 for both detection schemes), and the outcome is shown in Figure 3, where forward detection is characterized by a remarkable increase in the signal amplitude and, conversely, backward detection is distinguished by a significant signal reduction after a steep (but modest) increase similar to what is found for forward CARS. The different response of forward and backward CARS in dependence on

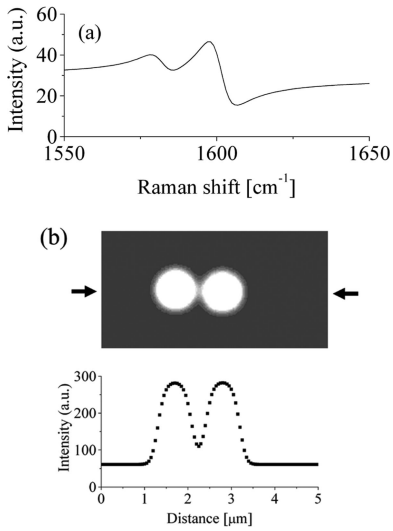

Figure 5. MicroCARS of polystyrene beads. (a) F-CARS spectrum based on eq 9. Physical and optical parameters are taken from Cheng et al. in ref 1. (b) Reconstruction of an image with two beads. The lateral intensity profile is shown below the image, and its baseline is chosen equal to the background appearing in the intensity profile of Figure 8b of ref 1. Note that peak shapes and contrast equal the experimental results of ref 1.

the sphere diameter is numerically calculated in the context of diffraction theory in Figure 4a of ref 1 (or the same figure indicated as Figure 6a in ref 2). This result is comparable with Figure 3 of the current work, and as regards the forward CARS only, one can see that significant discrepancies between the approximated calculation and the literature are not noticeable. More interestingly, the approximated curve for backward CARS adheres less to the result of diffraction theory, even though the expected initial increase followed by the oscillating decay is qualitatively retrieved. In particular, the oscillating behavior appearing between 0.5 and $2\lambda_p$ reproduces almost exactly the oscillations found in Figure 4a of ref 1, but the approximated signal decreases too rapidly when contrasted with what is reported for Raman samples of $D > 2\lambda_p$ illuminated with diffraction-limited laser beams. This happens because the role of diffraction becomes important for those experimental circumstances where the wave vector mismatch Δk is large. Since backward CARS of copropagating laser beams is characterized by the maximum absolute value of Δk, signal contributions from spatial sections of the Raman sample away from the focus plane are no longer negligible. In this condition, the influence of the main spatial peak at the microscope focus (see the example of Figure 1) is attenuated, and thus its wings with secondary peaks come back into play.

Other geometrical shapes of the Raman medium could be researched in addition to spheres. For example, integration over a cylinder implies that

$$b(\Theta) = \mathrm{Re}[\mathrm{Erf}(\xi)] \int_0^1 \eta J_0(k_{aS}\delta_1\eta \sin\Theta) \times \exp[-3(\delta_1\eta/w_g)^2]\, \mathrm{d}\eta \quad (11)$$

with $\xi = \sqrt{3}[\delta_2/z_g + iz_g\Delta k/6]$ and δ_1 and δ_2 indicating, respectively, the radius and the semilength of the cylinder. Equation 11 is very interesting because the integral can be solved analytically in terms of a series of hypergeometric functions (see the Supporting Information), and this results in the comparison of Figure 4. Here, the case of a rod, a sphere, and a disk of equal spatial volumes is provided under similar physical conditions to those in the work of Cheng et al.[1] As seen in their result (see Figure 3b of ref 1), the change in the geometrical structures of the anti-Stokes radiation is clearly visible.[22]

4. CARS Microscopy with a Gaussian Focus: Imaging

Next, as a last applicative example of possible uses of the 3DG approximation in the present context of microCARS, let us examine the crucial problem of image reconstruction, where the physical description is troubled by the displacement of the microscope focus with respect to the Raman-resonant source. In effect, two-dimensional or, even better, three-dimensional imaging is the final goal of any spectral application of CARS microscopy, but unfortunately, theoretical approach is beyond the reach of the picture given ordinarily in the established literature that imposes a common spatial origin for the frames of reference associated with the optical setup and the Raman medium, meaning that the resonant Raman source should be resident in the microscope focus.[1−4] On the contrary, the 3DG approximation can give a valid opportunity to control in an elegant way the spatial independence between the setup and the relevant CARS source. For instance, two-dimensional imaging of spheres becomes feasible if we calculate the anti-Stokes field relative to a displacement of the laser focus in the radial plane (x, y) indicated by the coordinates x_L and y_L. The result is summarized by the following set of equations (see Supporting Information),

$$\mathbf{E}_{aS}^{(q)}(\mathbf{R}) = -\frac{\sqrt{3}}{3}\pi^{3/2} S_q u_R z_g \delta^2 E_p^2(0)\, E_S^*(0)\, F(\Theta,\Phi)\, \mathbf{e}_q \quad (12)$$

$$F(\Theta,\Phi) = \exp[-(z_g\Delta k)^2/12]\, b(\Theta,\Phi) \quad (13)$$

$$b(\Theta,\Phi) = \exp\left[-3(x_L^2 + y_L^2)/w_g^2\right]\left[\chi_{nr}^{(3)} h_{nr} + (\chi_r^{(3)} - \chi_{nr}^{(3)}) h_r\right] \quad (14)$$

with the nonlinear susceptibility decomposed into its resonant ($\chi_r^{(3)}$) and nonresonant ($\chi_{nr}^{(3)}$) parts, whose interplay is determined by the functions $h_{nr} = w_g^2/(3\delta^2)\exp[(u^2 + v^2)/12]$ and $h_r = 2\sum_{m=0}^{\infty}\psi(m)[\delta^2(u^2 + v^2)/(4w_g^2)]^m/(m!)^2$, which, in turn, depend on the dimensionless variables u and v containing the important connection to the spatial coordinates, that is, $u = 6x_L/w_g - ik_{aS}w_g(\sin\Theta)(\cos\Phi)$ and $v = 6y_L/w_g - ik_{aS}w_g(\sin\Theta)(\sin\Phi)$. The coefficient $\psi(m)$ in h_r represents instead the sole contribution of numerical elaboration limited to the following integral

$$\psi(m) = \int_0^1 \eta^{2m+1} \exp[-3(\delta\eta/w_g)^2]\, \mathrm{Re}\{\mathrm{Erf}[\xi(\eta)]\}\, \mathrm{d}\eta \quad (15)$$

The examination of the equations characterizing the anti-Stokes field under the 3DG approximation shows that description of two-dimensional microCARS imaging is now much simpler than the complete treatment involving many numerical calculations necessary to cope with the loss of spatial symmetry.

To test the reliability of the approximation leading to eqs 12−15, we will consider polystyrene beads that are regarded as a model system useful in assessing the performance of CARS microscopy.[1−4] More precisely, taking as a reference the experimental results observed in Figure 8 of Cheng et al.,[1] or in Figure 10 of Cheng and Xie,[2] two are the Raman bands that are chosen to set up the current example. They appear at 1582 and 1601 cm^{-1}, and their lineshapes mimic what is spectrally expected for protein and DNA Raman bands.[1,2] The characteristics of a CARS spectrum of polystyrene beads are thus visible

in Figure 5a. The spectral curve has been calculated by taking into account the finite bandwidths of the laser beams,[23] and this result can now be used to build the image reported in Figure 5b containing two beads illuminated with pump and Stokes lasers being detuned of 1596 cm^{-1}. For instance, the comparison with the experimental results of Cheng et al., that is, Figure 8b of ref 1, suggests good agreement with the physical picture behind the current work.

5. Conclusions

In summary, the use of the 3DG approximation, which is very effective in fluorescence microscopy, seems to hold promise for interesting applications within the context of CARS microscopy. The main advantage lies in the easier theoretical characterization of the main microCARS features that have been clearly worked out for collinear and copropagating laser beams focused with an objective lens of high NA. However, the approach is not free from troubles consequent upon the approximation. Among them, the most relevant is the poor account of the interference effect taking place in the backward detection of CARS signals emitted by large Raman samples. Other inaccuracies are of minor importance and do not alter the good qualitative agreement with the results obtained under the complete numerical elaboration based on diffraction theory. In some cases, the agreement is also quantitatively acceptable. Where this does not happen, it should be recalled that conventional CARS theory is subjected to the arbitrariness of a multiplication factor (for instance, see the figures of refs 1 and 2 where calculated signals are given in terms of arbitrary units). In this manner, a suitable rescaling of the approximated results (that agree qualitatively with the corresponding results of diffraction theory) might become tolerable to match CARS intensities of the two approaches. In spite of this, the relevance of the present work is summarized by the analytical descriptions established for some basic shapes of Raman sources (i.e., small sphere, rod, disk). Furthermore, CARS correlation spectroscopy, understood so far under the assumption of completely phase-matched anti-Stokes signals[14,15] (implying some sort of spatial filtering to select with a small aperture the signal emitted in the direction of the complete phase matching), could be more generally reformulated in order to account for the dependence on the detection angle Θ that might lead to an alteration of the correlation amplitude and its decay. As a matter of fact, this dependence on the detection angle Θ is at the basis of CARS microscopy and is central to the features discussed in the present work, but it does not appear in the previous application of the 3DG approximation to CARS correlation spectroscopy.[14,15]

In conclusion, the approach is user-friendly and avoids the complications associated with heavy numerical calculation. The ultimate benefit of this simplification is demonstrated in section 4, where a simulation of microCARS imaging is reported with good correspondence to published experimental results. Considering this additional advantage, we can reasonably claim that the findings of the current research could be very helpful in strengthening the pivotal role played by CARS in biochemical microspectroscopy.

Acknowledgment. The support of L. Rivagum is acknowledged.

Supporting Information Available: Solution of the integral shown in eq 11 and complete mathematical derivation of eqs 12−14. This material is available free of charge via the Internet at http://pubs.acs.org.

References and Notes

(1) Cheng, J.-X.; Volkmer, A.; Xie, X. S. *J. Opt. Soc. Am. B* **2002**, *19*, 1363.
(2) Cheng, J.-X.; Xie, X. S. *J. Phys. Chem. B* **2004**, *108*, 827.
(3) Volkmer, A. *J. Phys. D: J. Appl. Phys* **2005**, *38*, R59.
(4) Müller, M.; Zumbusch, A. *ChemPhysChem* **2007**, *8*, 2156.
(5) Shen, Y. R. Principles of Nonlinear Optics; Wiley: New York, 1984.
(6) Duncan, M. D.; Reintjes, J.; Manuccia, T. J. *Opt. Lett.* **1982**, *7*, 350.
(7) Zumbusch, A.; Holtom, G. R.; Xie, X. S. *Phys. Rev. Lett.* **1999**, *82*, 4142.
(8) Lakowicz, J. R. *Topics in Fluorescence Spectroscopy. Vol. 1, Techniques*; Kluver Academic Publishers: New York, 2002.
(9) Gell, C.; Brockwell, D.; Smith, A. *Handbook of Single Molecule Fluorescence Spectroscopy*; Oxford University Press: Oxford, 2006.
(10) Rigler, R.; Elson, E. S. *Fluorescence Correlation Spectroscopy*; Springer: Berlin, 2001.
(11) Aragón, S. R.; Pecora, R. *J. Chem. Phys.* **1976**, *64*, 1791.
(12) Richards, B.; Wolf, E. *Proc. R. Soc. London A* **1959**, *253*, 358.
(13) Hess, S. T.; Huang, S.; Heikal, A. A.; Webb, W. W. *Biochemistry* **2002**, *41*, 697.
(14) Hellerer, T.; Schiller, A.; Jung, G.; Zumbusch, A. *ChemPhysChem* **2002**, *7*, 630.
(15) Cheng, J.-X.; Potma, E. O.; Xie, S. X. *J. Phys. Chem. A* **2002**, *106*, 8561.
(16) Cheng, J.-X.; Xie, X. S. *J. Opt. Soc. Am. B* **2002**, *19*, 1604.
(17) Marrocco, M. *Laser Physics* **2007**, *17*, 935.
(18) Note that such integrals contain exponentials with imaginary argument. This is in agreement with the original work of Richards and Wolf in ref 12, whereas the review by Cheng et al. in ref 1 presents exponentials with real arguments. This little glitch reappears in ref 16.
(19) Hess, S. T.; Webb, W. W *Biophys. J.* **2002**, *83*, 2300.
(20) Zipfel, W. R.; Williams, R. M.; Webb, W. W. *Nat. Biotechnol.* **2003**, *21*, 1369.
(21) Volkmer, A.; Cheng, J.-X.; Xie, X. S. *Phys. Rev. Lett.* **2001**, *87*, 23901.
(22) Unfortunately, the comparison between Figure 4 of this work and the corresponding result of refs 1 and 2 can only be qualitative. Quantitative considerations are prevented from a significant mistake in the evaluation of the volumes made on the basis of the geometrical parameters provided by Cheng et al. Although they declare that the different scatterers have the same volume, the sphere is 4 times bigger than the other types of Raman samples.
(23) Marrocco, M. *J. Raman Spectrosc.* **2007**, *38*, 1064.

JP805869S